

Simultaneous Spectral/Spatial Detection of Edges for Hyperspectral Imagery: The HySPADE Algorithm Revisited

Ronald G. Resmini¹

The MITRE Corporation
Kingstowne Center 4
5875 Barclay Drive, Suite 7, MS BELV
Alexandria, Virginia 22315

Abstract. The hyperspectral/spatial detection of edges (HySPADE) algorithm, originally published in 2004 [1], has been modified and applied to a wider diversity of hyperspectral imagery (HSI) data. As originally described in [1], HySPADE operates by converting the naturally two-dimensional edge detection process based on traditional image analysis methods into a series of one-dimensional edge detections based on spectral angle. The HySPADE algorithm: i) utilizes spectral signature information to identify edges; ii) requires only the spectral information of the HSI scene data and does not require a spectral library nor spectral matching against a library; iii) facilitates simultaneous use of all spectral information; iv) does not require endmember or training data selection; v) generates multiple, independent data points for statistical analysis of detected edges; vi) is robust in the presence of noise; and vii) may be applied to radiance, reflectance, and emissivity data—though it is applied to radiance and reflectance spectra (and their principal components transformation) in this report. HySPADE has recently been modified to use Euclidean distance values as an alternative to spectral angle. It has also been modified to use an N-pixel x N-pixel sliding window in contrast to the 2004 version which operated only on spatial subset image chips. HySPADE results are compared to those obtained using traditional (Roberts and Sobel) edge-detection methods. Spectral angle and Euclidean distance HySPADE results are superior to those obtained using the traditional edge detection methods; the best results are obtained by applying HySPADE to the higher-order, information-containing bands of principal components transformed data (both radiance and reflectance). However, in practice, both the Euclidean distance and spectral angle versions of HySPADE should be applied and their results compared. HySPADE results are shown; extensions of the HySPADE concept are discussed as are applications for HySPADE in HSI analysis and exploitation.

Keywords: edge detection, hyperspectral imagery, HSI, spatial, spectral, spectral angle, Euclidean distance, Roberts, Sobel

1. INTRODUCTION

There are relatively few algorithms for the simultaneous exploitation of the spatial and spectral information content of imaging spectrometer data. Early methods were developed for multispectral imagery (MSI). It is only within the last several years have existing techniques been expanded upon and new ones applied to hyperspectral imagery (HSI); see refs. [1-18]. It seems natural to assume that the capability to simultaneously utilize spatial and spectral information would enhance and even increase the information content mined from HSI. More specifically, the incorporation of edge information should improve the performance of algorithms for applications such as lines of communication (LOC) extraction, scene segmentation, automatic object mensuration, change detection, and vector content generation. The HySPADE algorithm provides a capability to exploit spectral information; i.e., information about material composition, to identify boundaries (edges) between different materials (spatial information). A version of HySPADE has been created that utilizes Euclidean distance; this new version, and the original which utilizes spectral angle, have been applied to additional visible/near infrared to shortwave infrared (VNIR/SWIR; 0.4 μm to 2.5 μm) HSI data cubes. These are extensions of the original work of [1].

HySPADE provides an under-utilized HSI exploitation product: a map of the transitions or boundaries between objects, materials, and backgrounds as they occur in a scene captured by a hyperspectral sensor. HySPADE edge-detected output resembles a blue-print of a scene; analysts and/or downstream algorithms in a processing chain are provided with an enhanced, clutter-removed, and segmented rendition of a scene. An analyst's attention is then drawn to those regions in the scene indicating changes in material composition. Identifying and characterizing material composition

¹ Author contact information: v: 703-470-3022 • f: 703-983-6989 • e₁: rresmini@mitre.org • e₂: rresmini@gmu.edu.

changes—e.g., vehicles on a concrete or asphalt parking lot, a chemical substance spilled on concrete, asphalt, or soil; a gravel road passing through a vegetated plain—form the core of the HSI information extraction process.

As will be discussed in the sections to follow, HySPADE: i) utilizes spectral information to identify edges; ii) requires only the spectral information of the HSI scene data and thus does not require a spectral library nor spectral matching against a library; iii) facilitates simultaneous use of all spectral information; iv) does not require endmember or training data selection; v) does not require band selection; vi) generates multiple, independent data points for statistical analysis of detected edges; vii) is robust in the presence of noise (see ref. [1]); viii) performs well when similarly colored objects occur in the imagery; and ix) may be applied to radiance, reflectance, and emissivity data and to principal components (or minimum noise fraction) transformed representations of those data types.

2. METHOD

The following discussion is taken largely from Resmini (2004) [1]. For clarity, this discussion will highlight the use of spectral angle; however, minimum Euclidean distance (MED) may be substituted for spectral angle for describing the functionality of the new Euclidean distance version of HySPADE. The HySPADE algorithm originally described in [1] is outlined in Figure 1. The HySPADE process begins with the input of an HSI data cube. The cube can be either calibrated at-aperture radiance, ground-leaving radiance (i.e., atmospherically corrected longwave infrared HSI), reflectance, or emissivity spectra. Here, at-aperture radiance and reflectance spectra are used. HySPADE is applied with a sliding window; window size is user-selectable. Generally, a 50 by 50-pixel window is sufficient. Within the $N \times N$ -pixel window, the $N \times N$ pixels are processed simultaneously without further sub-windowing or other spatial subsetting. The window is then advanced (also by a user-selectable quantity of pixels) and processing begins on the next block of N by N -pixel data. Sliding the window by N -pixels (where N is the window dimension in one direction) is also sufficient (and decreases computation time) and is employed in the data analyses presented below².

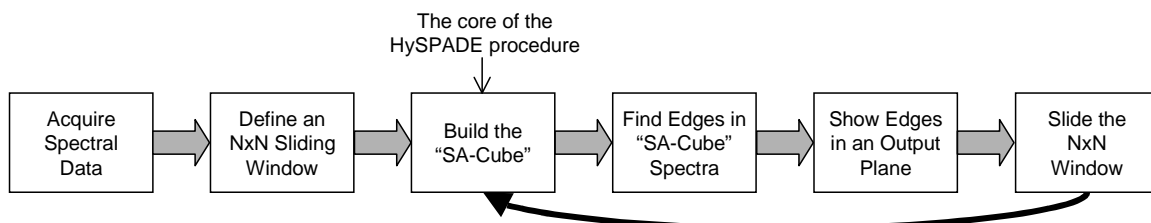


Figure 1: The general process flow for HySPADE (SA = spectral angle). Euclidean distance may be substituted for spectral angle (see text).

The second box of Figure 2 describes the core of the HySPADE process. An intermediate cube (actually a cubelet) called the spectral angle (SA) cube is constructed by applying the spectral angle mapper (SAM) algorithm with each pixel in the $N \times N$ -pixel window with each and every other pixel in the same window. In other words, band 1 of the intermediate SA cube contains the spectral angle of the spectrum in pixel location [sample 1, line 1] of the window with every other spectrum in the window. Band 2 of the SA cube contains the spectral angle of the spectrum in pixel location [1,2] with every other spectrum in the original cube. And so on. The intermediate SA cube is depicted in the third box of Figure 2; it has dimensions of N samples by N lines by N^2 bands and each pixel is a spectrum of spectral angle values in radians.

A 'spectrum' from this intermediate SA cube contains information about changes in composition of materials as they occur within the window (i.e., spectral and spatial information). For example, consider a window encompassing four different materials with four different spectra. Further, the window is comprised of these four materials each occurring as discrete blocks in succession (see [1] and [23]). The spectrum from the [1,1] position in the SA cube would contain four plateaus separated by three abrupt boundaries or edges between these plateaus; the SA cube spectrum is recording

² Actually, the window is translated $N-2$ pixels. The lag of two pixels mitigates the impact of an edge effect of HySPADE. This is discussed in a later section.

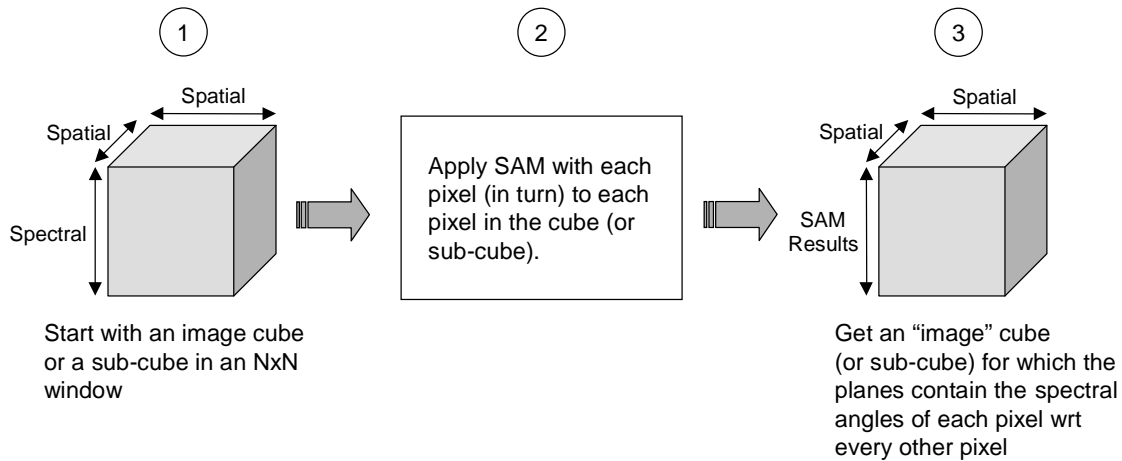


Figure 2: The first three processing steps of HySPADE (wrt = with respect to). Euclidean distance may be substituted for spectral angle (see text).

the fact that within the window there are four different materials. The 'band number' of the SA-cube spectrum is easily translated into the original window [sample, line] address. Thus, the 'band number' of the boundaries in the SA cube spectrum yields the [sample, line] pixel coordinate of the edge in the window.

The spectra of the SA cube are then analyzed, each in turn, for edge detection. In other words, one (or more) traditional one-dimensional edge detection techniques are applied to the one-dimensional data of each SA cube spectrum. A first-order finite-difference is used in HySPADE; more robust techniques may be employed. Again, the SA cube spectrum band number corresponds to pixel address; i.e., [sample, line], in the original window. Thus, when an edge is detected in the analysis of an SA cube spectrum, the 'band number' of the edge is converted to the [sample, line] address in the N by N -pixel window and a point is plotted (actually a running tally is incremented; see below) on a separate output plane indicating the presence of the edge. Note that HySPADE thus converts a two-dimensional, single plane-based, kernel-based edge detection problem into a series of one-dimensional edge detection processes. A user-defined threshold (or range of thresholds) is used to interpret the one-dimensional edge detection results. More discussion about this threshold is provided later.

Figure 3 indicates that as soon as an edge is detected in the analysis of a single SA cube spectrum it is recorded/tallied in an output plane. HySPADE has been applied in this mode. However, since every SA cube 'spectrum' contains similar edge location information (derived, however, with a different spectrum), edges may be decided upon following accumulation of the information contained in every SA cube spectrum. Statistical techniques may then be applied for the final edge location determination and for producing estimates of the probability of correct edge location and/or combined with the spatial sampling modulation transfer function (MTF) of the sensor to refine edge location. These are topics for additional investigation and are beyond the scope of the present report.

The process described above must be applied twice to the HSI data in the window: once traversing the window in the row-wise direction and again traversing the data in the column-wise sense.

A post-processing step to exclude the first row and the first column (or last row, last column depending on direction of traversal across the original HSI data) of the $N \times N$ -pixel window is required to counteract a wrap-around artifact in the algorithm. This does not, in any way, hamper the performance of the algorithm. Indeed, to incorporate excluded data and get the full performance of HySPADE, the sliding window could be moved by, e.g., $N-2$ pixels (the default currently implemented in HySPADE). Other strategies may also be possible.

The HySPADE edge-detection plane records a tally, on a pixel-by-pixel basis, of the number of times a given [sample, line] address is indicated as an edge by the one-dimensional edge detection process (i.e., the first-order finite-difference) applied to each SA cube spectrum. An edge for a given [sample, line] address is tallied if the value of the first-order

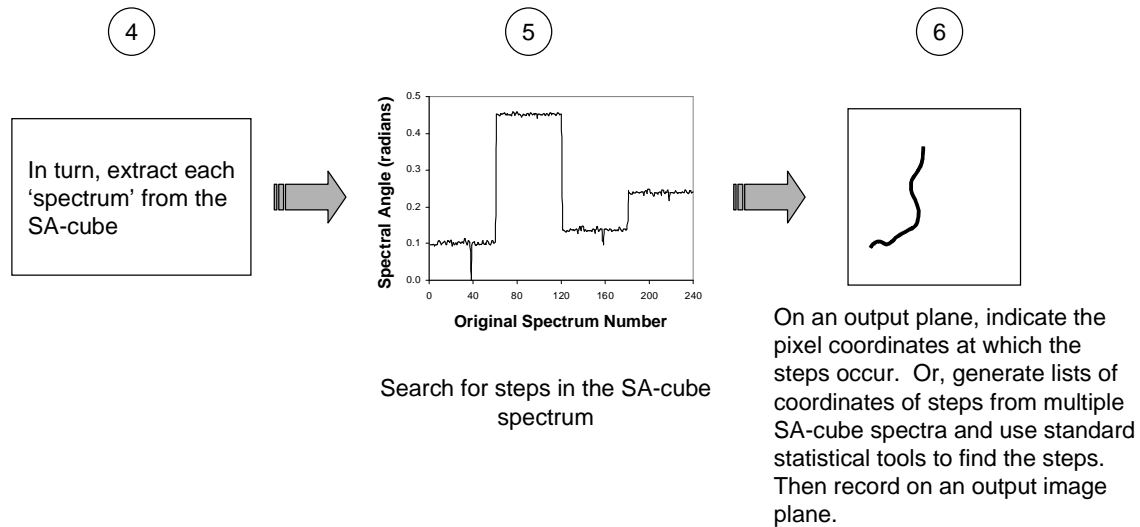


Figure 3: Steps four through six of the HySPADE process. The SA cube spectra contain the edge detection information. If Euclidean distance is substituted for spectral angle, then the Euclidean distance cube (or MED cube) spectra will contain the edge detection information. See [1] and [17] for the simulated data set from which the SA cube spectrum is drawn.

finite-difference process generates a value exceeding a user-selected threshold (for positive finite-difference values) or generates a value less than the negative of the same user-selected threshold (for negative finite-difference values). The threshold currently used is defined as a multiple of the standard deviation (e.g., 0.20σ , 0.40σ , 0.80σ , 1.00σ) of the first-order finite-difference edge detection values calculated from each SA cube spectrum³. In actuality, HySPADE outputs twenty planes each representing twenty different thresholds (based on standard deviation). The start is 0.20σ and increments by 0.20σ . The number of output planes and the σ -increment are also user selectable.

The HySPADE edge-detection planes are then imported into an image processing system and displayed individually. Since a plane contains a range of pixel values (i.e., the edge tallies), its presentation as an image may subsequently be enhanced using histogram stretching (and/or other image enhancement techniques).

Spectral angle HySPADE is applied to VNIR/SWIR HSI at-aperture radiance and reflectance cubes and their principal component transformations.

2.1 HySPADE with Euclidean Distance

A new version of HySPADE has been created that employs minimum Euclidean distance (MED) instead of spectral angle. All of the preceding discussion applies to this version of the algorithm; the functionality is identical except that spectral angle value is replaced by Euclidean distance. Spectral angle will highlight spectral differences without regard for illumination or overall brightness differences amongst pixels of the same material type. Euclidean distance, on the other hand, will emphasize spectral as well as brightness differences.

The Euclidean distance version of HySPADE is also applied to VNIR/SWIR HSI at-aperture radiance and reflectance cubes and their principal component transformations.

2.2 HySPADE with Modeled Data

The application of HySPADE to a simulated HSI data cube (with noise) is given in refs. [1] and [17] and will not be repeated here.

³A global σ value may be utilized rather than the current (and preferred) implementation of calculating σ on an SA-cube-spectrum by SA-cube-spectrum basis.

2.3 Applying the Roberts and Sobel Edge Detectors to the HSI Data

Commercially available software is used to apply the Roberts and Sobel edge detection methods to the HSI data. Specifically, the Roberts convolution is applied to every band individually in an image cube generating n edge detection output planes where n is the number of bands in the input cube. These results, the n edge detection planes, are then summed to yield a single edge detection output plane (there are other combination strategies). Upon display as a grayscale image, this single output plane may be manipulated via its image histogram. The same procedure is then applied using the Sobel edge detector.

3. SOFTWARE AND TOOLS

HySPADE is currently implemented as engineering code in the C programming language. The code has been compiled and run with Microsoft Visual C++ 2010 Express Edition on a personal computer workstation running Microsoft Windows 7. User interfacing is by a DOS command prompt window; a windowed graphical user interface (GUI) has not yet been created but is a goal of ongoing development. The ENVI[®] v4.7 software package was used for data preparation (e.g., spatial subsetting, bad/noisy band removal, principal components transformation), visualization, thresholding, and additional analyses such as the Roberts and Sobel edge-detection filtering.

4. THE HYPERSPECTRAL DATA

Airborne VNIR/SWIR HSI data of Reno, NV, acquired on September 13, 2006, with the Prospectir sensor are analyzed with HySPADE. The data are freely available via web access; see ref. [22]. Calibrated radiance data were converted to apparent reflectance by SpecTIR, the data provider; noisy bands and bands in those portions of the spectrum impacted by atmospheric water vapor are removed. The radiance data are 320 samples by 600 lines by 322 bands; the reflectance data are 320 samples by 600 lines by 350 bands; both data types range in wavelength from 0.42 μm to 2.44 μm with band full-width at half-maxima ranging from 0.00570 μm to 0.00870 μm . Additional information about the data and SpecTIR's processing methods may be found at [22]. A near-infrared false color composite of the data is shown in Figure 4.



Figure 4. A near-infrared false color composite image (red: 0.86 μm ; green: 0.64 μm ; blue: 0.55 μm) of the Reno, NV, Prospectir VNIR/SIR HSI data.

5. RESULTS

Figures 5 through 8 show HySPADE results; Figures 9 and 10 show the results of the Roberts edge detector applied as described above. Sobel edge detection results are essentially identical, visually, to those of Roberts and are not shown here but may be seen at [23]. Each figure caption indicates the data type to which each method was applied (i.e., radiance, reflectance, or principal components [PC] transformed versions of these), the threshold for which the image corresponds (for the HySPADE results), and the stretch used to display the image (2% linear or arbitrarily selected to best depict, subjectively, the edge detection results). All HySPADE results were produced with a 50 by 50-pixel

window. For PC-transformed data, HySPADE and Roberts are applied to a subset of the bands corresponding to the first 30 or first 10 component images as indicated in the respective figure captions. Results of the various methods applied to the full PC-transformed data cubes may also be seen at [23].



Figure 5. Spectral angle (SA) HySPADE, 50x50-pixel window, radiance data, 0.40σ , 2% linear stretch.



Figure 6. Spectral angle (SA) HySPADE, 50x50-pixel window, reflectance data, 1.40σ , arbitrarily stretched.



Figure 7. Spectral angle (SA) HySPADE, 50x50-pixel window, 1st 30 bands of the PC-transformed reflectance data, 1.00σ , 2% linear stretch.



Figure 7. Minimum Euclidean distance (MED) HySPADE, 50x50-pixel window, reflectance data, 1.00σ , 2% linear stretch.



Figure 8. Minimum Euclidean distance (MED) HySPADE, 50x50-pixel window, 1st 10 PC-transformed bands of the reflectance data, 0.80σ , 2% linear stretch.



Figure 9. Roberts, sum of all bands, reflectance data, 2% linear stretch. Roberts, mean of all reflectance bands, also with a 2% linear stretch, is indistinguishable and is not shown here. The Sobel results are very similar to those of Roberts and are not shown here but may be seen at [23].



Figure 10. Roberts, sum of 1st 30 bands of the PC-transformed reflectance data, 2% linear stretch.

6. DISCUSSION

6.1 HySPADE Performance.

As evident in the figures above, the quality of HySPADE results varies according to the data type to which the algorithm is applied. HySPADE (both the spectral angle and Euclidean distance versions) accurately capture edge information when applied to at-aperture radiance data, reflectance data, and to their principal components (PC) transformations⁴. HySPADE output is also more evenly toned when displayed with a 2% linear stretch. In general, edges erode in each successive HySPADE output plane (i.e., from 0.20σ to 4.0σ). The best performance, however, is obtained with spectral angle HySPADE applied to PC transformed radiance and reflectance data (Figure 7); the edge lines are thinner and provide an excellent indication of edge locations. The results are visually similar whether the entire PC cube or the first 30 PC images are processed. The relative noisiness of the lower order PC images evidently does not impact HySPADE's edge detection performance. These results suggest applying a PC transformation to an HSI data set and then applying HySPADE to a subset of the PC image planes (the higher-order PC images) to obtain good edge detection with a minimum of computation time. HySPADE (spectral angle and Euclidean distance) applied directly to at-aperture radiance also produces excellent edge detection results. Particularly with VNIR/SWIR HSI, perhaps the best strategy to pursue for edge detection is the application of HySPADE, the spectral angle and Euclidean distance versions, to at-aperture radiance data and to PC transformed at-aperture radiance (with a full set of PC images and then with a subset). This strategy parallels that of applying numerous edge detectors to panchromatic images such as Roberts, Sobel, Prewitt, and directional (to highlight various orientations).

HySPADE responds to compositional changes by utilizing the full spectral signature; it is not a technique that responds simply to illumination/brightness/gray scale differences on a band-by-band basis. Spectral angle HySPADE utilizes all of the capability of spectral angle mapping with spectral signature information and is insensitive to brightness/albedo differences. Euclidean distance HySPADE also responds to spectral signature differences as well as to differences in brightness/albedo of those signatures.

6.1.1 Thresholding HySPADE Results.

As described above, a HySPADE output plane is a tally, on a pixel-by-pixel basis, of the number of times a given [sample, line] address is indicated as an edge by the one-dimensional edge detection process applied to each SA or MED spectrum. An edge for a given [sample, line] address is tallied if the value of the first-order finite-difference process generates a value exceeding a threshold. The current implementation of HySPADE outputs twenty planes each representing twenty different thresholds (from 0.20σ to 4.0σ by 0.20σ). The analyst may view and modify the output planes individually via their histograms thus providing more options for defining, selecting, and refining edges. This is

⁴ It is worth noting that spectral angle HySPADE applied to PC transformed data is essentially the adaptive coherence/cosine estimation (ACE) algorithm.

in contrast to the Roberts (and Sobel) results as generated for this study for which only one output plane is produced (and which may also be modified with its histogram). Alternatively, the n bands of the Roberts (or Sobel or other edge detectors) results may be analyzed individually where n is equal to the number of bands in the original HSI cube; however, this would be quite inefficient from the analyst's perspective. The twenty HySPADE output planes, and the ability to interact with their histograms, provide more information and more flexibility to interpret and assess edge detection results.

HySPADE results may also be viewed using ENVI[®]'s animation feature. This facilitates observing edges erode (and dilate in the reverse animation sequence) as a function of threshold. Indeed, erosion or dilation algorithms may be applied as post-processing.

6.1.2 Different Window Sizes.

HySPADE window size was varied in increments of 10 from 30 x 30 to 70 x 70-pixels. In general, as window size decreases, computation time decreases. There are minor but notable differences in performance particularly as window size gets very small. There is a processing artifact that may be mitigated if spectral angle or MED threshold values are selected with respect to their noise equivalent quantities (e.g., noise equivalent spectral angle). HySPADE will attempt to define an edge where one may not exist within a compositionally homogeneous expanse in the imagery that is larger than the window size. This may be resolved by checking whether the range of angle or MED values is equal to their respective noise equivalent quantities. This has not yet been incorporated in HySPADE. A detailed analysis of the edge detection performance as a function of window size is beyond the scope of the present report but is an area of ongoing work.

6.1.3 Comparison with Roberts and Sobel.

The Roberts and Sobel results are quite good and are obtained rapidly requiring very little computation time. HySPADE lines, however, seem qualitatively crisper (and are, in fact, better defined for the PC transformed data) and with more even gray tones than those of Roberts and Sobel. Further, the texture of the HySPADE results—particularly in those regions where there are many closely juxtaposed edges with a wide range of orientations—is a better representation of the distribution of materials (and edges and compositional complexity) in the original image though in some instances is less line drawing-like. Not creating a line where there may not actually be one is perhaps a desirable quality of an edge-detection technique. Stated alternatively, high spatial frequency changes in compositional complexity may yield HySPADE results that are textured rather and blue-print like in the rendering of edges. When processing one band at a time, Roberts, Sobel, and other traditional edge detectors may not be so impacted but may fail to detect (or hint at the presence of) different materials present in a scene. Such performance characteristics of the various edge detection algorithms suggests their usage in combination.

As evident in Figure 10, Roberts applied to PC-transformed cubes produces rather unsatisfactory results. Similar results are obtained for the Sobel edge detector applied to PC transformed data. Noise artifacts are enhanced (a line artifact in the lower half of Figure 10 is evident) and there is a salt-and-pepper appearance to the results due to large pixel-to-pixel changes in the Roberts output values.

6.2 Unprocessed Columns.

The current implementations of the HySPADE codes (both spectral angle and Euclidean distance) leave a few columns on the right and a few lines at the bottom of an HSI image cube unprocessed. These data are then displayed with zeros and appear as a black vertical rectangle appended to the right-hand side and a black horizontal rectangle appended to the bottom of the edge detection planes. This is an artifact based on chosen window size and the number of pixels the window is translated between iterations. These null areas are cropped away prior to display in this report. Future versions of HySPADE (particularly those with a more sophisticated GUI) should be designed to inform and assist the user with parameter selection to maximize scene area processed and minimize (and actually eliminate) unprocessed image columns and rows.

6.3 Subpixel Objects.

The simultaneous use of spatial and (all) spectral information may also reveal subpixel objects. This is perhaps best demonstrated when small objects are emplaced as part of a controlled collection experiment (or for data for which there

is ground-truth). An example of this is given in Figure 9 of ref. [1]. Without reliable ground-truth information, it is difficult to point to an example in the results shown here.

6.4 Computation Time.

HySPADE is computationally intensive; Roberts and Sobel (as applied here to HSI data) are much less so. With Roberts and Sobel, results are obtained rapidly (in seconds) whereas HySPADE requires up to several minutes, depending on window size. Computation time may be decreased if HySPADE is applied only to the first n (with n arbitrarily chosen by the analyst) principal component (or minimum noise fraction) images. Computation time also decreases significantly when window size is decreased. Other strategies for decreasing computation time are also possible (but not implemented in the current HySPADE codes). E.g., calculate edge locations with every n^{th} (also a possible user-defined parameter) SA cube or MED cube spectrum since each such spectrum contains edge location information for the entire $N \times N$ -pixel window within which it was calculated. Alternatively (or in addition), build the SA or MED cube with every n^{th} pixel in the original $N \times N$ -pixel window.

6.5 HySPADE for Automatic Endmember Extraction.

HySPADE may be applied as a pre-processor for automatic endmember finder algorithms. HySPADE's output highlights one category of likely mixed pixels: the edges and perhaps a one pixel buffer zone around them. Almost certainly this definition of mixed pixel would be sensitive to sensor ground sample distance (GSD). The expanses between edges are compositionally homogeneous (although they may be some form of mixture as well; e.g., vegetation plus soil but manifesting as a discrete class). Utilizing HySPADE output, an endmember finder would simply have to search for those regions or patches of all zeros because the edges (ostensibly encompassing the mixed pixels in the scene) have responses greater than zero. I.e., mask out the edges prior to providing an HSI cube to, e.g., the N-FINDR [25], pixel purity index (PPI) [26], SMACC [24], etc., endmember finder algorithms.

The area under the curve (AUC) of the HySPADE output—the tally vs. σ —will also indicate pixels that are likely edges. Large AUC values indicate edges; low values indicate non-edge, compositionally homogeneous pixels. Thus, to locate areas of compositionally homogeneous materials, one possible strategy is to search for regions of zero value in the individual HySPADE output planes (particularly those corresponding to higher σ thresholds) combined with low AUC values in plots of tally vs. σ for individual pixels.

6.6 True Simultaneous Spectral/Spatial Processing.

As shown in the figures in Section 5, HySPADE accurately captures edge information. The simultaneous use of spatial and spectral information for edge detection removes the need to select those bands to which edge detection will be applied. HySPADE also mitigates the need for strategies to combine individual edge detection planes encountered when traditional approaches to edge detection are applied to imaging spectrometer (HSI and MSI) data. In the search for edges in an HSI cube, HySPADE robustly exploits spectral information; indeed, the HySPADE method is more akin to traditional information extraction techniques utilized for the analysis and exploitation of HSI data. HySPADE also utilizes all of the spectral signature variability inherent in an HSI cube.

6.7 Measures of Effectiveness (MOEs).

HySPADE, as currently implemented, simply tallies edge coordinates as soon as they are determined during the analysis of each individual SA or MED cube spectrum. Confidence in edge detection is not estimated. MOEs for detected edges are, however, hypothetically calculable⁹. Recall that each spectrum in an SA or MED cube contains edge information derived from different spectra in the original HSI input window providing different, independent estimates of edge locations. Thus, the edge detection analysis of all SA or MED cube spectra (prior to deciding edge locations) should generate a population of edge coordinate estimates which may then be analyzed with statistical methods and/or combined with the spatial MTF of the sensor to refine edge location.

7. SUMMARY

An algorithm for hyperspectral edge detection was presented. The HySPADE method simultaneously utilizes spectral and spatial information to identify edges. Attributes and benefits of the HySPADE method include the utilization of spectral information to identify edges; the simultaneous use of spatial and spectral information; and applicability to radiance, reflectance, and emissivity data. HySPADE edge-detection may be used in the analysis and exploitation of

HSI for applications such as lines of communication (LOC) extraction, scene segmentation, automatic object mensuration, edge-information change-detection, and vector content generation. HySPADE results were compared to those obtained using the traditional Roberts and Sobel edge-detection methods. More information on HySPADE and the HySPADE code are available at [23].

8. FUTURE DIRECTIONS

Several possible enhancements to (and research for) HySPADE include: i) incorporating the method Sweet (2003) [20], a combination of the spectral angle and Euclidean distance algorithms for greater separation of spectral signatures; ii) incorporating techniques other than the first-order finite-difference currently used in HySPADE for the main edge detection processing; iii) investigating the use of (and optimum combination of) multiple edge detection algorithms (e.g., HySPADE --> Canny [19] --> etc.) for improved edge detection-based HSI exploitation; iv) comparing HySPADE performance with additional traditional edge-detection methods; v) applying HySPADE (spectral angle, Euclidean distance) to minimum noise fraction (MNF) transformed hyperspectral (and multispectral) imagery data; vi) testing various window sizes: 50x50, 40x40, 20x20, 10x10-pixel and various increments of window translation between iterations; vii) developing a graphical user interface; viii) applying line thinning (eroding) and/or line connecting/line tracing (see, e.g., [21]) to HySPADE output to close gaps and to generate an output plane that more closely resembles a line drawing or blueprint of a scene; ix) incorporating measures of effectiveness /figures of merit for edge detection results based on the numerous, independent edge detections generated by the HySPADE method; x) investigate the impact on edge detection using trimmed/outlier-removed statistics estimated from the first-order one-dimensional finite difference calculations; and xi) conduct computation time benchmarking.

REFERENCES

1. Resmini, R.G., (2004). Hyperspectral/Spatial Detection of Edges (HySPADE): An algorithm for spatial and spectral analysis of hyperspectral information. Proceedings of the SPIE, Algorithms and Technologies for Multispectral, Hyperspectral, and Ultraspectral Imagery X, S.S. Shen and P.E. Lewis, eds., Orlando, Fla., April 12-16, v. 5429, doi: 10.1117/12.541877, pp. 433-442.
2. Landgrebe, D.A., (2003). *Signal Theory Methods in Multispectral Remote Sensing*. Wiley Series in Remote Sensing and Image Processing, John Wiley & Sons, New Jersey, 508 p.
3. Van der Werff, H., Van Ruitenbeek, F., Van der Meijde, M., Van der Meer, F., De Jong, S., and Kalubandara, S., (2007). Rotation-Variant Template Matching for Supervised Hyperspectral Boundary Detection. *IEEE Geoscience and Remote Sensing Letters*, v. 4, no. 1, pp. 70-74.
4. Theiler, J., and Gisler, G. (1997). A contiguity-enhanced k-means clustering algorithm for unsupervised multispectral image segmentation. In: Proceedings of the SPIE, v. 3159, pp. 108-118.
5. Keshavarz, A., and Ghassemian, H., (2008). Hyperspectral classification using Markov random field and spatial probability density function. *International Symposium on Telecommunications*, pp. 677-681.
6. Bass, D., (2008). Enhanced line detection using hyperspectral data. *Journal of Applied Remote Sensing*, v. 2, pp. 1-10.
7. Benediktsson, J., Palmason, J., and Sveinsson, J., (2005). Classification of hyperspectral data from urban areas based on extended morphological profiles. *IEEE Transactions on Geoscience and Remote Sensing*, v. 43, no. 3, pp. 480-491.
8. Noyel, G., Angulo, J., and Jeulin, D., (2007). Morphological segmentation of hyperspectral images. *Image Analysis and Stereology*, v. 26, pp. 101-109.
9. Plaza, A., Marinez, P., Perez, R., and Plaza, J., (2002). Spatial/spectral endmember extraction by multidimensional morphological operations. *IEEE Transactions on Geoscience and Remote Sensing*, v. 40, no. 9, pp. 2025-2041.

10. Plaza, A., Plaza, J., and Martin, G., (2009). Incorporation of spatial constraints into spectral mixture analysis of remotely sensed hyperspectral data. *IEEE International Workshop on Machine Learning for Signal Processing*, pp. 1-6.
11. Bakker, W., and Schmidt, K., (2002). Hyperspectral edge filtering for measuring homogeneity of surface cover types. *ISPRS Journal of Photogrammetry and Remote Sensing*, v. 56, no. 4, pp. 246-256.
12. Zortea, M., and Plaza, A., (2009). Spatial preprocessing for endmember extraction. *IEEE Transactions on Geoscience and Remote Sensing*, v. 47, no. 8, pp. 2679-2693.
13. Luo, B., and Chanussot, J., (2009). Hyperspectral image classification based on spectral and geometrical features. *Proceedings of the IEEE*, 6 p.
14. Fauvel, M., Benediktsson, J.A., Chanussot, J., and Sveinsson, J.R., (2008). Spectral and spatial classification of hyperspectral data using SVMs and morphological profile. *IEEE Transaction on Geoscience and Remote Sensing*, v. 46, no. 11, pp. .
15. Palmason, J.A., Benediktsson, J.A., Sveinsson, J.R., and Chanussot, J., (2005). Classification of hyperspectral data from urban areas using morphological preprocessing and independent component analysis. In *IEEE IGARSS '05 International Geoscience and Remote Sensing Symposium*, Seoul Korea, pp. 176-179.
16. Martin, G., and Plaza, A., (2010). Spatial-spectral preprocessing for volume-based endmember extraction algorithms using unsupervised clustering. *Proceedings of the IEEE*, 4 p.
17. Rogge, D.M., Rivard, B., Zhang, J., Sanchez, A., Harris, J., and Feng, J., (2007). Integration of spatial-spectral information for the improved extraction of endmembers. *Remote Sensing of Environment*, v. 110, no. 3, pp. 287-303.
18. Stocker, A.D., Reed, I.S., and Yu, X., (1990). Multi-dimensional signal processing for electro-optical target detection. In: *Signal and Data Processing of Small Targets 1990*, *Proceedings of the SPIE*, v. 1305, pp. 218-231.
19. Canny, J., (1986). A computational approach to edge detection. *IEEE Transactions on Pattern Analysis and Machine Intelligence*, v, 8, no. 6, pp. 679-698.
20. Sweet, J.N., (2003). The spectral similarity scale and its application to the classification of hyperspectral remote sensing data. In: *Advances in Techniques for Analysis if Remotely Sensed Data*, *IEEE Workshop*, v. 27-28, pp. 92-99.
21. Line tracing tools include Adobe Illustrator CSX Live Trace; see, e.g., <http://www.adobe.com/designcenter/illustrator/articles/illcs2bglvtrace/illcs2bglvtrace.pdf>; and tracing in GIMP; see, e.g., <http://www.gimpusers.com/tutorials/making-a-pencil-drawing-from-a-photo> and <http://registry.gimp.org/files/plugin-trace-notes.txt> and http://www.gimphelp.org/autotrace_manual.shtml and <http://autotrace.sourceforge.net/>.
22. Information about SpecTIR, the Prospectir sensor, the Reno, NV, data, and SpecTIR's data processing may be found at: <http://www.spectir.com/>, <http://www.spectir.com/airbornesurveys.html>, <http://www.spectir.com/download.html>, and <http://www.spectir.com/assets/Text%20Files/Calibration%20and%20Data%20Processing%20Overview.pdf> all last accessed on Feb. 8, 2012.
23. Additional information on HySPADE may be found at: http://mason.gmu.edu/~rresmini/HySPADE_SPIE_2012.html.

24. Gruninger, J., Ratkowski, A.J., and Hoke, M.L., (2004). The Sequential Maximum Angle Convex Cone (SMACC) Endmember Model. In: Proceedings of the SPIE, Algorithms for Multispectral and Hyper-spectral and Ultraspectral Imagery, S.S. Shen and P.E. Lewis, eds., v. 5425-1, Orlando FL, April, 2004.
25. Winter, M.E., (1999). N-FINDR: an algorithm for fast autonomous spectral end-member determination in hyperspectral data. In Proceedings of the SPIE, Imaging Spectrometry V, M.R. Descour, S.S. Shen, eds., v. 3753, no. 266, <http://dx.doi.org/10.1117/12.366289>.
26. Boardman, J.W., Kruse, F.A., and Green, R.O., (1995). Mapping target signatures via partial unmixing of AVIRIS data. In Summaries, Fifth JPL Airborne Earth Science Workshop, JPL Publication 95-1, v. 1, pp. 23-26.